Editors' Suggestion | Featured in Physics

Twist Angle-Dependent Interlayer Exciton Lifetimes in van der Waals Heterostructures

Junho Choi,[1] Matthias Florian,[2] Alexander Steinhoff,[2] Daniel Erben,[2] Kha Tran,[1] Dong Seob Kim,[1] Liuyang Sun,[1] Jiamin Quan,[1] Robert Claassen,[1] Somak Majumder,[3] Jennifer A. Hollingsworth,[3] Takashi Taniguchi,[4] Kenji Watanabe,[5] Keiji Ueno,[6] Akshay Singh,[7] Galan Moody,[8] Frank Jahnke,[2] and Xiaoqin Li[1,*]

[1]*Department of Physics and Center for Complex Quantum Systems, The University of Texas at Austin, Austin, Texas 78712, USA*
[2]*Institute for Theoretical Physics, University of Bremen, 28334 Bremen, Germany*
[3]*Materials Physics & Applications Division: Center for Integrated Nanotechnologies, Los Alamos National Laboratory, Los Alamos, New Mexico 87545, USA*
[4]*International Center for Materials Nanoarchitectonics, National Institute for Materials Science, 1-1 Namiki, Tsukuba, Ibaraki 305-0044, Japan*
[5]*Research Center for Functional Materials, National Institute for Materials Science, 1-1 Namiki, Tsukuba, Ibaraki 305-0044, Japan*
[6]*Department of Chemistry, Graduate School of Science and Engineering, Saitama University, Saitama, 338-8570, Japan*
[7]*Department of Physics, Indian Institute of Science, Bengaluru, Karnataka 560012, India*
[8]*Department of Electrical and Computer Engineering, University of California Santa Barbara, Santa Barbara, California 93106, USA*

(Received 8 May 2020; revised 13 November 2020; accepted 4 December 2020; published 26 January 2021)

In van der Waals (vdW) heterostructures formed by stacking two monolayers of transition metal dichalcogenides, multiple exciton resonances with highly tunable properties are formed and subject to both vertical and lateral confinement. We investigate how a unique control knob, the twist angle between the two monolayers, can be used to control the exciton dynamics. We observe that the interlayer exciton lifetimes in $MoSe_2/WSe_2$ twisted bilayers (TBLs) change by one order of magnitude when the twist angle is varied from 1° to 3.5°. Using a low-energy continuum model, we theoretically separate two leading mechanisms that influence interlayer exciton radiative lifetimes. The shift to indirect transitions in the momentum space with an increasing twist angle and the energy modulation from the moiré potential both have a significant impact on interlayer exciton lifetimes. We further predict distinct temperature dependence of interlayer exciton lifetimes in TBLs with different twist angles, which is partially validated by experiments. While many recent studies have highlighted how the twist angle in a vdW TBL can be used to engineer the ground states and quantum phases due to many-body interaction, our studies explore its role in controlling the dynamics of optically excited states, thus, expanding the conceptual applications of "twistronics".

DOI: 10.1103/PhysRevLett.126.047401

Van der Waals (vdW) heterostructures offer a unique material platform with rich electronic and optical properties highly tunable via a wide selection of layer composition, strain, electric gating, and doping [1]. Because the lattice matching restriction is lifted at the interface, the twist angle between two monolayers (MLs) has emerged as a unique control knob to engineer the moiré superlattice formed by periodic variations of atomic alignment between the two layers [2,3]. Following exciting discoveries in graphene twisted bilayers (TBLs) [4–6], transition metal dichalcogenide (TMD) TBLs have also been found to exhibit rich correlated electronic phases [7–10]. In a different context, the lateral confinement introduced by the moiré potential may be used to realize a regular array of quantum emitters, a long-standing goal in the field of solid-state quantum information technology [11,12].

A type-II band alignment is typically found in a TMD TBL [Fig. 1(a)], leading to the formation of both intralayer and interlayer excitons [13–17]. We focus on interlayer excitons (IXs) because they are most likely to experience a deep moiré potential confinement. Because of the similar lattice constants of $MoSe_2$ and WSe_2 MLs, the size of the moiré supercell is determined by the twist angle [Fig. 1(b)]. The twist angle in real space translates into a rotation in the momentum space, causing the relative rotation of Brillouin zones associated with each monolayer [Fig. 1(c)]. Consequently, valleys in each layer are shifted from each other, changing a direct optical transition near the K valley to an indirect transition, introducing longer IX lifetimes [14,18]. We illustrate the exciton center of mass wave function in its own reference frame (i.e., the Γ point) in the excitation picture of Fig. 1(d). In TBLs with small twist angles ($\Theta < 5°$), the thermally broadened IX distribution is sufficient to satisfy the momentum conservation requirement of an indirect transition, allowing the radiative decay process. A wide range of IX lifetimes in TMD TBLs have been reported in time-resolved photoluminescence (TRPL) measurements previously [14,15,19–24]. However, no prior studies have explained the origin of such variations.

We perform TRPL measurements on a series of $MoSe_2/WSe_2$ TBLs with accurately controlled twist

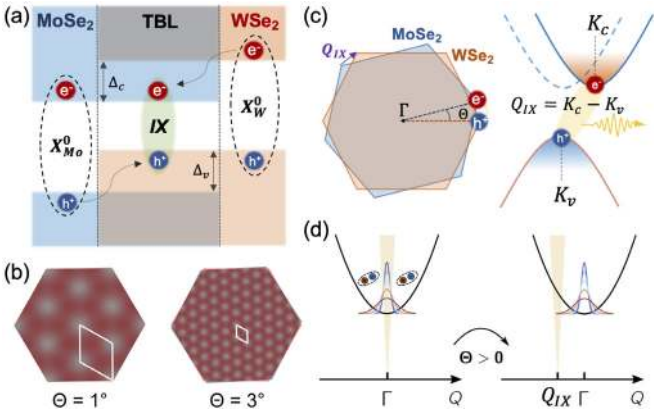

FIG. 1. Conceptual description of IXs in a TBL. (a) Schematic of type-II band alignment with band offsets (Δ_c and Δ_v) and interlayer charge transfer lead to the formation of IXs. (b) Real-space representation of the moiré superlattice for twist angles of 1° and 3° with a moiré supercell marked in white. (c) Schematic of the Brillouin zone of $MoSe_2$ ML (blue) and WSe_2 ML (orange) twisted in the momentum space (left panel). $Q_{IX} = K_c - K_v$ denotes a finite momentum mismatch between the two layers and corresponds to the center of mass momentum of IXs. This twist leads to an indirect transition (right panel). (d) Thermal distribution of IXs with a near-zero (left) and a finite (right) twist angle plotted in the exciton's reference frame. Blue (red) curve illustrates the thermal distribution of IXs at a low (high) temperature. Yellow shaded region illustrates the light cone.

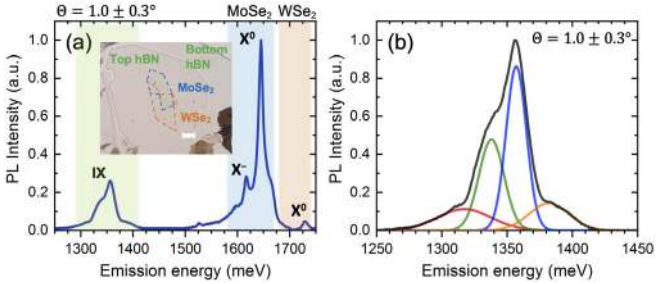

FIG. 2. (a) Low-temperature PL spectrum from a $MoSe_2/WSe_2$ TBL with $\Theta = 1.0 \pm 0.3°$ twist angle, featuring both intralayer excitons (neutral exciton: X^0, trion: X^-) and IXs. Inset shows the optical image of the hBN-encapsulated TBL. $MoSe_2$ and WSe_2 ML regions are indicated inside the blue and orange dashed lines, respectively. Scale bar: 20 μm (b) Gaussian fitting to multiple IXs. Black solid line is measured data.

angles. And we observe that the IX lifetime changes by one order of magnitude when the twist angle is changed from 1° to 3.5°. Theoretically, we examine two mechanisms that influence the IX radiative lifetimes. We find that both the shift to indirect optical transition with an increasing twist angle and the moiré potential have a significant effect on the lifetime. Our theory further predicts that IX lifetimes exhibit different temperature dependence in TBLs with different twist angles. This prediction is partially validated by the experimental observations.

The hexagonal boron nitride (hBN) encapsulated TBLs are prepared using a standard exfoliation and stacking procedure described in the Supplemental Material (SM) [25,26]. The twist angle is estimated from high-resolution optical microscopy images, and the stacking type of the TBLs is determined by second-harmonic generation (SHG) (see SM for details) [27–30]. All optical experiments are performed using an averaged excitation power of 1 μW and a focused laser spot size of $\sim$1 μm in diameter. Our far-field experiment probes hundreds of moiré supercells simultaneously. The data represent statistical averages of an ensemble of excitons. We present the low-temperature PL spectrum from the TBL with $\Theta = 1.0 \pm 0.3°$ twist angle in Fig. 2(a), in which both IXs and intralayer exciton resonances with large binding energy of a few hundred meV are observed [14–16,31–34]. We fit multiple IX resonances in the PL spectrum by Gaussian functions as shown in Fig. 2(b). We present the PL spectra for the other two samples with different twist angles, and the analysis of the multiple IX resonances with consistent dielectric environments in the SM [35,36]. Different possible interpretations for these resonances have been proposed, including phonon-mediated states, defect-bound states, and spin triplet states [37–40]. While we cannot rule out these alternative explanations definitively, we find that the interpretation of quantized exciton resonances confined within the moiré potential captures the essential features of our data as we further explain below [12,15,41].

The recombination dynamics of IXs in three TBLs are spectrally and temporally resolved at low temperatures as shown in Figs. 3(a)–3(c). The TRPL signals are fitted with a biexponential decay function. Such a biexponential decay indicates that a simple two-level model is not sufficient to explain the dynamics of IXs. This biexponential decay may originate from scattering between a bright and dark exciton [42–44]. Using a rate equation analysis for a three-level system (see SM for details, which includes Refs. [45–48]), we attribute the fast (slow) decay component to the lifetime of the bright (dark) exciton assuming the scattering rate between the bright and dark state is slower than the bright exciton lifetime. In all samples, we observe shorter IX lifetimes as the energy of the resonance increases as shown in the inset to each panel in Figs. 3(a)–3(c). This systematic change with energy is consistent with the interpretation that the higher energy excitons are excited states in the moiré potential with additional relaxation channels [15]. The reduced exciton lifetimes associated with the excited states are often found in spatially localized excitons in other materials [49].

Most remarkably, the IX lifetime changes drastically as a function of the twist angle, as shown in Fig. 3(d). Both the fast and slow components of the IX lifetime increase nearly by one order of magnitude when the twist angle increases from $\Theta = 1°$ to 3.5°. For example, the fast (slow) decay time measured over the range of 1345–1355 meV increases from 1.3 (6.6) to 16.2 (217.5) ns. We focus on

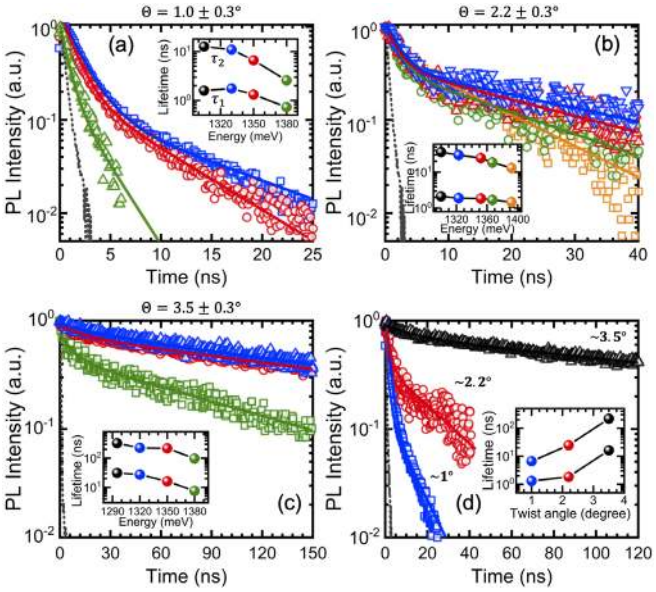

FIG. 3. Twist angle dependent lifetimes of all IX resonances measured from (a) $\Theta = 1.0 \pm 0.3°$, (b) $2.2 \pm 0.3°$, and (c) $3.5 \pm 0.3°$ TBLs, respectively. Inset shows the energy dependence of the fast (τ_1) and slow (τ_2) decay components of IX lifetimes. Solid and black dotted lines represent fitting with a biexponential decay and instrumental response functions, respectively. (d) Twist angle dependence of IX lifetimes measured near 1345–1355 meV in the TBLs. Inset summarizes the extracted fast and slow decay components in the three TBLs.

understanding this twist angle dependence of IX lifetimes in TBLs.

To understand this drastic twist angle dependence, we calculate the radiative recombination rate of IXs in the TBLs (see the SM for details, which includes Refs. [23,50–57]). We note that the lifetime measured is in fact the total lifetime, determined by both radiative and nonradiative processes. It is impractical to calculate all nonradiative processes, which may depend on many extrinsic properties. Thus, our calculations can only be compared to ideal emitters with unity quantum yield. Nevertheless, these calculations provide important understanding of IX dynamics controlled by the twist angle in a TBL and guide the search for more efficient emitters in a moiré crystal. Our calculations start with Fermi's golden rule [58]

$$\tau_{\mathrm{IX}}^{-1} = \frac{2\pi}{\hbar}\sum_{if}|\langle f|H_{\mathrm{rad}}|i\rangle|^2\delta(\varepsilon_i - \varepsilon_f)N_i \tag{1}$$

where the optical matrix element describes transitions between the initial IX state $|i\rangle$ and the final photon state $|f\rangle = b^\dagger_{\mathbf{q},\sigma}|0\rangle$. Here, $b^\dagger_{\mathbf{q},\sigma}$ creates a photon with wave vector $\mathbf{q}$ and polarization σ with respect to the vacuum state $|0\rangle$, and N_i is the occupation of the initial IX states. To describe the moiré exciton states we use a low energy continuum model that we derive along the lines of Refs. [11,12,18,59]. As the basis of describing the hybridized IXs later, we have first written the wave function of IXs in the absence of interlayer coupling as

$$|\mathbf{Q}\rangle = \frac{1}{\sqrt{\mathcal{A}}}\sum_{\mathbf{k}}\phi_X(\mathbf{k})a^{\dagger,c}_{\mathbf{K}_c+\mathbf{k}+(m_e/M)\mathbf{Q}}a^{v}_{\mathbf{K}_v+\mathbf{k}-(m_h/M)\mathbf{Q}}|0\rangle \tag{2}$$

with eigenenergies $E(\mathbf{Q}) = \hbar^2|\mathbf{Q}|^2/(2M) + E_{\mathrm{gap}} - E_B$ that are characterized by the center-of-mass momentum $\mathbf{Q}$. Here, $a^{\dagger,c}_{\mathbf{K}_c+\mathbf{q}}(a^{v}_{\mathbf{K}_v+\mathbf{q}})$ creates (annihilates) an electron in the K_c (K_v) valley of the conduction (valence) band, $M = m_e + m_h$ is the total exciton mass, and m_e (m_h) is the electron (hole) effective mass. $\mathcal{A}$ is the crystal area. The electron-hole relative-motion wave function in momentum space $\phi_X(\mathbf{k})$ is determined by the Wannier equation. Its solution determines the IX energy $E_{\mathrm{gap}} - E_B$, where E_B is the IX binding energy and E_{gap} is the band gap.

An interlayer twist in real space generates a relative shift in momentum space [$\mathbf{K}_c - \mathbf{K}_v$, see Fig. 1(c)] as well as a spatial modulation of the exciton energy. In all three TBLs, the moiré periodicity can be assumed to be large compared to the IX Bohr radius. Thus, we neglect the variation of the binding energy in the moiré pattern and use a local approximation of the IX moiré potential $V^M(\mathbf{R})$ according to Ref. [12]. In this framework, the IX Hamiltonian reads

$$H = -\frac{\hbar^2}{2M}\Delta_{\mathbf{R}} + V^M(\mathbf{R}), \tag{3}$$

where $-(\hbar^2/2M)\Delta_{\mathbf{R}}$ is the exciton center-of-mass kinetic energy and can be diagonalized using a plane-wave expansion with eigenenergies $\varepsilon_{\mathbf{Q},\lambda}$ and eigenstates

$$|\mathbf{Q},\lambda\rangle = \sum_{\mathbf{G}_M} c^{\lambda}_{\mathbf{Q}-\mathbf{G}_M}|\mathbf{Q}-\mathbf{G}_M\rangle. \tag{4}$$

The moiré reciprocal lattice vectors $\mathbf{G}_M$ are derived as differences of top and bottom layer reciprocal lattice vectors. Therefore, the size of the moiré Brillouin zone (MBZ) scales with the interlayer twist angle. We represent its center and boundary by γ and κ, respectively. We use the above plane-wave expansion, and solve the optical matrix element between the initial moiré exciton state $|\mathbf{Q},\lambda\rangle$ and the final photon state $|\mathbf{q},\sigma\rangle$. Moiré excitons can only recombine if the momentum conservation law $\mathbf{Q} - \mathbf{q}_{\|} = \mathbf{K}_c - \mathbf{K}_v := \mathbf{Q}_{\mathrm{IX}}$ is fulfilled where $\mathbf{q}_{\|}$ represents the in-plane component of the photon wave vector. We assume that the twist angle is sufficiently large so that typical photon momenta are still small compared to the MBZ, which in our case is well justified for twist angles larger than 0.5°. In this case, we can discard umklapp processes.

In the numerical calculation shown in Fig. 4, we assume the exciton population is thermalized obeying a Boltzmann distribution. To clarify the twist angle dependence, we

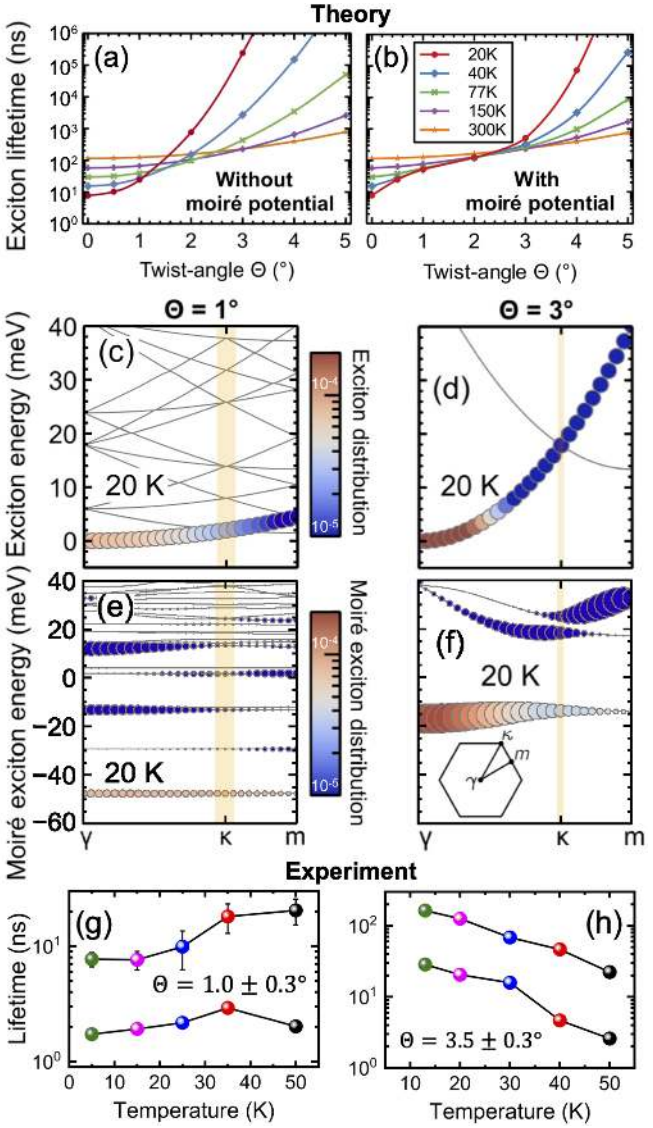

FIG. 4. Temperature and twist angle dependence of calculated IX radiative lifetimes in the absence and presence of a moiré potential and measured temperature dependent IX dynamics. Calculated twist angle dependence of the IX lifetimes shown for various temperatures in the (a) *absence* and (b) *presence* of a moiré potential. Panels (c) and (d) show the IX band structure in the *absence* of a moiré potential at twist angles of $\Theta = 1°$ and $\Theta = 3°$, respectively. Moiré exciton states are classified by momenta from the first MBZ shown in inset of (f). The light cone (orange shaded area) occupies a larger fraction of the MBZ for a TBL with a smaller twist angle. Panels (e) and (f) show the moiré exciton band structure, thermal distribution, and density-of-states contribution for different twist angles at low-temperature. Scale of the symbol size is the same for panels (c),(d) and (e),(f). Note that at small twist angle the IX bands become flat due to the moiré potential. (g),(h) Measured temperature dependent fast and slow decay components of lifetimes near 1350 meV in the TBLs with $\Theta = 1.0 \pm 0.3°$ ($3.5 \pm 0.3°$) from 5 to 50 K (13 to 50 K). Error bars are smaller than the symbols for some data points.

disentangle the influence of the valley shift in reciprocal space from the energy modulation of moiré potential. First of all, a drastic change in IX lifetimes with the twist angle is expected even in the absence of a moiré potential by just considering the shifted valleys illustrated in Figs. 1(c) and 1(d). Only excitons within the light cone can decay radiatively. For a TBL with a small twist angle, low temperatures are favorable to thermally keep as many excitons as possible within a narrow region around the Γ point in the excitation picture. On the other hand, in a TBL with a large twist angle, light-matter coupling benefits from long tails in the high-temperature exciton distribution to overcome the large momentum shift Q_{IX}. As a result, the temperature dependence of IX lifetimes exhibits opposite behavior in TBLs with small and large twist angles. We therefore predict a crossover between these two regimes around an intermediate twist angle of $\theta = 2°$ as shown in Fig. 4(a).

Figures 4(c) and 4(d) provide detailed insight for the cases of small and large twist angles at low temperature, showing that at small twist angle the light cone overlaps with more occupied exciton states. Because of the absence of a moiré potential, the parabolic dispersion is simply folded back to the first MBZ without hybridization of bands. In Fig. 4(b), the presence of a moiré potential does not change the general trends but leads to a softening of the twist angle dependence. This can be understood as the moiré potential introducing an interaction between the IXs with different center-of-mass momenta as represented by the matrix form of Eq. (3). Thereby, the momentum conservation between the IX and photon in the light-matter coupling process is relaxed, opening additional channels for radiative recombination, as shown in Figs. 4(e) and 4(f). Correspondingly, the IX bands become less dispersive due to the moiré potential. Nevertheless, the IX lifetimes are predicted to change by several orders of magnitude when the twist angle is tuned between 1° and 3.5°. Here, the symbol size quantifies the contribution of the moiré exciton states to the bright density of states as given by the coefficients $c^{\lambda}_{\mathbf{Q}}$ in Eq. (4). Comparing panels (e) and (f), we see that a small twist angle is particularly beneficial for light emission at low temperatures due to the flattening of IX bands that leads to strong population of κ excitons. We further compare the moiré exciton distribution at 20 K [Fig. 4(f)] and 300 K (SM, Fig. S5b), demonstrating how a thermally broadened IX distribution fosters exciton-photon coupling at a large twist angle. In all cases, we find that higher excitonic bands become occupied due to the moiré-induced mixture of bands represented by the relevant ($G_M = 0$) contributions [$c^{\lambda}_{\mathbf{Q}}$ in Eq. (4) as shown in Figs. 4(e) and 4(f)], in contrast to the cases when the moiré potential is not taken into account in Figs. 4(c) and 4(d).

To examine the predicted temperature dependence of IX radiative lifetimes, we compare measurements performed on two TBLs with the caveat that the total lifetime is measured. Figures 4(g) and 4(h) show the temperature dependent two decay times extracted by fitting with a biexponential function for the two TBLs with $\Theta = 1°$ and 3.5°, respectively. Indeed, we experimentally observed opposite trends in the temperature dependent IX lifetimes in two TBLs. The IX lifetime increased (decreased) at higher temperature in the small (large) twist angle sample. This trend is consistent with the calculation [Fig. 4(b)] although a much weaker temperature dependence was observed. The deviation of the fast lifetime component from the $\Theta = 1°$ sample at ~50 K may originate from increased phonon-mediated nonradiative processes.

We discuss the scope and limitations of our studies. First, we focus on $MoSe_2/WSe_2$ TBLs with relatively small twist angles with a more accurate angle control than most previous experiments that have investigated the change of exciton resonances over a broader range of twist angle [60–63]. In TBLs with a small twist angle, the thermal distribution of the IX may be sufficient to satisfying the momentum conservation requirements of an indirect optical transition. In practice, phonon-assisted transitions do exist. Such transitions play an increasingly important role in TBLs with larger twist angle ($\Theta > 5°$). Second, the biexponential decay dynamics are not fully explained. We provide a rate equation analysis for a three-level system involving a dark state in the SM. Such a dark state may originate from an indirect transition involving electrons or holes in a different valley. Third, our calculations only address the radiative decay rate and our experiments measure the total decay rate. The calculation models an ideal situation where the IX dynamics is determined by the radiative process with unity quantum yield. It addresses the question of how radiative decay can be controlled by the twist angle with and without the presence of an moiré superlattice. The qualitative agreement between the experiments and calculations is noteworthy. This agreement may suggest that the nonradiative decay processes either do not depend on the twist angle strongly or depend on the twist angle in a similar way as the radiative decay.

In conclusion, our studies represent a first step toward understanding how the twist angle of a vdW heterostructure can be used to control exciton dynamics. These results provide critical guidance to efforts on searching for exciton condensates where a long IX lifetime is preferred to reach an equilibrium temperature with the lattice. On the other hand, light-emitting devices should be built with TMD TBLs with a small twist angle. A faster radiative lifetime can compete favorably with other nonradiative processes and lead to higher quantum efficiency. Our work introduces new methods, "momentum-space band shift" and "periodic in-plane energy modulation," for controlling exciton lifetimes. These methods may be adapted by researchers investigating different classes of materials and be exploited by a wide variety of optoelectronic devices.

We gratefully acknowledge the helpful discussions with Kyounghwan Kim, Yimeng Wang, Wooyoung Yoon, and Emanuel Tutuc for sample preparation. The spectroscopic experiments performed by J. C. at UT-Austin and X. Li were primarily supported by NSF DMR-1808042. The support for K. T. was provided by the NSF MRSEC program DMR-1720595. Authors at UT-Austin acknowledge the use of facilities and instrumentation supported by the National Science Foundation through the Center for Dynamics and Control of Materials: an NSF MRSEC under Cooperative Agreement No. DMR-1720595. Material preparation was funded by the Welch Foundation via Grant No. F-1662. R. C. was supported by NSF EFMA-1542747. K. W. and T. T. acknowledge support from the Elemental Strategy Initiative conducted by the MEXT, Japan, Grant No. JPMXP0112101001, JSPS KAKENHI Grant No. JP20H00354, and the CREST(JPMJCR15F3), JST. K. U. acknowledges support from the JSPS KAKENHI Grant No. 25107004. S. M. was funded for developing new CdSe architectures by the U.S. Department of Energy division of Energy Efficiency and Renewable Energy (EERE), Grant No. M615002955. Work was performed in part at the Center for Integrated Nanotechnologies, a DOE, OBES Nanoscale Science Research Center & User Facility, with aspects of the work supported by a CINT User Project No. 2017BRA0033. G. M. acknowledges support by the NSF Quantum Foundry through Q-AMASE-i program Award No. DMR-1906325. The theoretical calculations performed by M. F., A. S., D. E. and F. J. were supported by the Deutsche Forschungsgemeinschaft (RTG 2247 "Quantum Mechanical Materials Modelling"). A. S. acknowledges funding from Indian Institute of Science start-up grant.

J. C. and M. F. contributed equally to this work.

*Corresponding author.
elaineli@physics.utexas.edu

[1] K. S. Novoselov, A. Mishchenko, A. Carvalho, and A. H. Castro Neto, Science **353**, aac9439 (2016).
[2] Y. Liu, N. O. Weiss, X. Duan, H.-C. Cheng, Y. Huang, and X. Duan, Nat. Rev. Mater. **1**, 16042 (2016).
[3] J. Quan, L. Linhart, M.-L. Lin, D. Lee, J. Zhu, C.-Y. Wang, W.-T. Hsu, J. Choi, J. Embley, C. Young, T. Taniguchi, K. Watanabe, C.-K. Shih, K. Lai, A. H. MacDonald, P.-H. Tan, F. Libisch, and X. Li, arXiv:2009.10650.
[4] Y. Cao, V. Fatemi, A. Demir, S. Fang, S. L. Tomarken, J. Y. Luo, J. D. Sanchez-Yamagishi, K. Watanabe, T. Taniguchi, E. Kaxiras, R. C. Ashoori, and P. Jarillo-Herrero, Nature (London) **556**, 80 (2018).
[5] Y. Cao, V. Fatemi, S. Fang, K. Watanabe, T. Taniguchi, E. Kaxiras, and P. Jarillo-Herrero, Nature (London) **556**, 43 (2018).

[6] K. Kim, A. DaSilva, S. Huang, B. Fallahazad, S. Larentis, T. Taniguchi, K. Watanabe, B. J. LeRoy, A. H. MacDonald, and E. Tutuc, Proc. Natl. Acad. Sci. U.S.A. **114**, 3364 (2017).

[7] Y. Tang, L. Li, T. Li, Y. Xu, S. Liu, K. Barmak, K. Watanabe, T. Taniguchi, A. H. MacDonald, J. Shan, and K. F. Mak, Nature (London) **579**, 353 (2020).

[8] E. C. Regan, D. Wang, C. Jin, M. I. Bakti Utama, B. Gao, X. Wei, S. Zhao, W. Zhao, Z. Zhang, K. Yumigeta, M. Blei, J. D. Carlström, K. Watanabe, T. Taniguchi, S. Tongay, M. Crommie, A. Zettl, and F. Wang, Nature (London) **579**, 359 (2020).

[9] Y. Shimazaki, I. Schwartz, K. Watanabe, T. Taniguchi, M. Kroner, and A. Imamoğlu, Nature (London) **580**, 472 (2020).

[10] L. Wang, E.-M. Shih, A. Ghiotto, L. Xian, D. A. Rhodes, C. Tan, M. Claassen, D. M. Kennes, Y. Bai, B. Kim, K. Watanabe, T. Taniguchi, X. Zhu, J. Hone, A. Rubio, A. N. Pasupathy, and C. R. Dean, Nat. Mater. **19**, 861 (2020).

[11] H. Yu, G.-B. Liu, J. Tang, X. Xu, and W. Yao, Sci. Adv. **3**, e1701696 (2017).

[12] F. C. Wu, T. Lovorn, and A. H. MacDonald, Phys. Rev. B **97**, 035306 (2018).

[13] J. Kang, S. Tongay, J. Zhou, J. Li, and J. Wu, Appl. Phys. Lett. **102**, 012111 (2013).

[14] P. Rivera, J. R. Schaibley, A. M. Jones, J. S. Ross, S. Wu, G. Aivazian, P. Klement, K. Seyler, G. Clark, N. J. Ghimire, J. Yan, D. G. Mandrus, W. Yao, and X. Xu, Nat. Commun. **6**, 6242 (2015).

[15] K. Tran *et al.*, Nature (London) **567**, 71 (2019).

[16] K. L. Seyler, P. Rivera, H. Yu, N. P. Wilson, E. L. Ray, D. G. Mandrus, J. Yan, W. Yao, and X. Xu, Nature (London) **567**, 66 (2019).

[17] E. M. Alexeev, D. A. Ruiz-Tijerina, M. Danovich, M. J. Hamer, D. J. Terry, P. K. Nayak, S. Ahn, S. Pak, J. Lee, J. I. Sohn, M. R. Molas, M. Koperski, K. Watanabe, T. Taniguchi, K. S. Novoselov, R. V. Gorbachev, H. S. Shin, V. I. Fal'ko, and A. I. Tartakovskii, Nature (London) **567**, 81 (2019).

[18] H. Yu, Y. Wang, Q. Tong, X. Xu, and W. Yao, Phys. Rev. Lett. **115**, 187002 (2015).

[19] P. Rivera, K. L. Seyler, H. Y. Yu, J. R. Schaibley, J. Q. Yan, D. G. Mandrus, W. Yao, and X. D. Xu, Science **351**, 688 (2016).

[20] B. Miller, A. Steinhoff, B. Pano, J. Klein, F. Jahnke, A. Holleitner, and U. Wurstbauer, Nano Lett. **17**, 5229 (2017).

[21] P. Nagler, M. V. Ballottin, A. A. Mitioglu, F. Mooshammer, N. Paradiso, C. Strunk, R. Huber, A. Chernikov, P. C. M. Christianen, C. Schuller, and T. Korn, Nat. Commun. **8**, 1551 (2017).

[22] L. A. Jauregui, A. Y. Joe, K. Pistunova, D. S. Wild, A. A. High, Y. Zhou, G. Scuri, K. De Greve, A. Sushko, C.-H. Yu, T. Taniguchi, K. Watanabe, D. J. Needleman, M. D. Lukin, H. Park, and P. Kim, Science **366**, 870 (2019).

[23] J. Wang, J. Ardelean, Y. Bai, A. Steinhoff, M. Florian, F. Jahnke, X. Xu, M. Kira, J. Hone, and X. Y. Zhu, Sci. Adv. **5**, eaax0145 (2019).

[24] J. Choi, W.-T. Hsu, L.-S. Lu, L. Sun, H.-Y. Cheng, M.-H. Lee, J. Quan, K. Tran, C.-Y. Wang, M. Staab, K. Jones, T. Taniguchi, K. Watanabe, M.-W. Chu, S. Gwo, S. Kim, C.-K. Shih, X. Li, and W.-H. Chang, Sci. Adv. **6**, eaba8866 (2020).

[25] A. Castellanos-Gomez, M. Buscema, R. Molenaar, V. Singh, L. Janssen, H. S. J. van der Zant, and G. A. Steele, 2D Mater. **1**, 011002 (2014).

[26] See Supplemental Material at http://link.aps.org/supplemental/10.1103/PhysRevLett.126.047401 for sample preparation, additional measurements, a rate equation analysis, and further details about the moire exciton lifetime calculations.

[27] N. Kumar, S. Najmaei, Q. Cui, F. Ceballos, P. M. Ajayan, J. Lou, and H. Zhao, Phys. Rev. B **87**, 161403(R) (2013).

[28] L. M. Malard, T. V. Alencar, A. P. M. Barboza, K. F. Mak, and A. M. de Paula, Phys. Rev. B **87**, 201401(R) (2013).

[29] Y. Li, Y. Rao, K. F. Mak, Y. You, S. Wang, C. R. Dean, and T. F. Heinz, Nano Lett. **13**, 3329 (2013).

[30] W. T. Hsu, Z. A. Zhao, L. J. Li, C. H. Chen, M. H. Chiu, P. S. Chang, Y. C. Chou, and W. H. Chang, ACS Nano **8**, 2951 (2014).

[31] N. R. Wilson, P. V. Nguyen, K. Seyler, P. Rivera, A. J. Marsden, Z. P. L. Laker, G. C. Constantinescu, V. Kandyba, A. Barinov, N. D. M. Hine, X. Xu, and D. H. Cobden, Sci. Adv. **3**, e1601832 (2017).

[32] M.-H. Chiu, M.-Y. Li, W. Zhang, W.-T. Hsu, W.-H. Chang, M. Terrones, H. Terrones, and L.-J. Li, ACS Nano **8**, 9649 (2014).

[33] A. Chernikov, T. C. Berkelbach, H. M. Hill, A. Rigosi, Y. Li, O. B. Aslan, D. R. Reichman, M. S. Hybertsen, and T. F. Heinz, Phys. Rev. Lett. **113**, 076802 (2014).

[34] M. M. Ugeda, A. J. Bradley, S.-F. Shi, F. H. da Jornada, Y. Zhang, D. Y. Qiu, W. Ruan, S.-K. Mo, Z. Hussain, Z.-X. Shen, F. Wang, S. G. Louie, and M. F. Crommie, Nat. Mater. **13**, 1091 (2014).

[35] I. C. Gerber and X. Marie, Phys. Rev. B **98**, 245126 (2018).

[36] A. Raja, L. Waldecker, J. Zipfel, Y. Cho, S. Brem, J. D. Ziegler, M. Kulig, T. Taniguchi, K. Watanabe, E. Malic, T. F. Heinz, T. C. Berkelbach, and A. Chernikov, Nat. Nanotechnol. **14**, 832 (2019).

[37] M. Danovich, D. A. Ruiz-Tijerina, R. J. Hunt, M. Szyniszewski, N. D. Drummond, and V. I. Fal'ko, Phys. Rev. B **97**, 195452 (2018).

[38] L. Zhang, R. Gogna, G. W. Burg, J. Horng, E. Paik, Y.-H. Chou, K. Kim, E. Tutuc, and H. Deng, Phys. Rev. B **100**, 041402(R) (2019).

[39] A. Ciarrocchi, D. Unuchek, A. Avsar, K. Watanabe, T. Taniguchi, and A. Kis, Nat. Photonics **13**, 131 (2019).

[40] W. Li, X. Lu, S. Dubey, L. Devenica, and A. Srivastava, Nat. Mater. **19**, 624 (2020).

[41] S. Brem, C. Linderälv, P. Erhart, and E. Malic, Nano Lett. **20**, 8534 (2020).

[42] G. Moody, J. Schaibley, and X. Xu, J. Opt. Soc. Am. B **33**, C39 (2016).

[43] M. Palummo, M. Bernardi, and J. C. Grossman, Nano Lett. **15**, 2794 (2015).

[44] X.-X. Zhang, Y. You, Shu Yang Frank Zhao, and T. F. Heinz, Phys. Rev. Lett. **115**, 257403 (2015).

[45] P. A. Dalgarno, J. M. Smith, B. D. Gerardot, A. O. Govorov, K. Karrai, P. M. Petroff, and R. J. Warburton, Phys. Status Solidi A **202**, 2591 (2005).

[46] Y. Chen, J. Vela, H. Htoon, J. L. Casson, D. J. Werder, D. A. Bussian, V. I. Klimov, and J. A. Hollingsworth, J. Am. Chem. Soc. **130**, 5026 (2008).
[47] C. J. Hanson, M. R. Buck, K. Acharya, J. A. Torres, J. Kundu, X. Ma, S. Bouquin, C. E. Hamilton, H. Htoon, and J. A. Hollingsworth, ACS Appl. Mater. Interfaces **7**, 13125 (2015).
[48] N. J. Orfield, S. Majumder, J. R. McBride, F. Yik-Ching Koh, A. Singh, S. J. Bouquin, J. L. Casson, A. D. Johnson, L. Sun, X. Li, C.-K. Shih, S. J. Rosenthal, J. A. Hollingsworth, and H. Htoon, ACS Nano **12**, 4206 (2018).
[49] A. Steinhoff, H. Kurtze, P. Gartner, M. Florian, D. Reuter, A. D. Wieck, M. Bayer, and F. Jahnke, Phys. Rev. B **88**, 205309 (2013).
[50] G.-B. Liu, W.-Y. Shan, Y. Yao, W. Yao, and D. Xiao, Phys. Rev. B **88**, 085433 (2013).
[51] M. Florian, M. Hartmann, A. Steinhoff, J. Klein, A. W. Holleitner, J. J. Finley, T. O. Wehling, M. Kaniber, and C. Gies, Nano Lett. **18**, 2725 (2018).
[52] N. A. Asriyan, I. L. Kurbakov, A. K. Fedorov, and Y. E. Lozovik, Phys. Rev. B **99**, 085108 (2019).
[53] M. A. Semina, Phys. Solid State **61**, 2218 (2019).
[54] I. Kylänpää and H.-P. Komsa, Phys. Rev. B **92**, 205418 (2015).
[55] R. Geick, C. H. Perry, and G. Rupprecht, Phys. Rev. **146**, 543 (1966).
[56] N. S. Rytova, Proc. MSU, Phys., Astron. **3**, 30 (1967).
[57] L. V. Keldysh, Sov. J. Exp. Theor. Phys. Lett. **29**, 658 (1979).
[58] A. Esser, E. Runge, R. Zimmermann, and W. Langbein, Phys. Rev. B **62**, 8232 (2000).
[59] F. Wu, T. Lovorn, and A. H. MacDonald, Phys. Rev. Lett. **118**, 147401 (2017).
[60] A. M. van der Zande, J. Kunstmann, A. Chernikov, D. A. Chenet, Y. You, X. Zhang, P. Y. Huang, T. C. Berkelbach, L. Wang, F. Zhang, M. S. Hybertsen, D. A. Muller, D. R. Reichman, T. F. Heinz, and J. C. Hone, Nano Lett. **14**, 3869 (2014).
[61] P. K. Nayak, Y. Horbatenko, S. Ahn, G. Kim, J.-U. Lee, K. Y. Ma, A. R. Jang, H. Lim, D. Kim, S. Ryu, H. Cheong, N. Park, and H. S. Shin, ACS Nano **11**, 4041 (2017).
[62] J. Kunstmann, F. Mooshammer, P. Nagler, A. Chaves, F. Stein, N. Paradiso, G. Plechinger, C. Strunk, C. Schüller, G. Seifert, D. R. Reichman, and T. Korn, Nat. Phys. **14**, 801 (2018).
[63] W.-T. Hsu, B.-H. Lin, L.-S. Lu, M.-H. Lee, M.-W. Chu, L.-J. Li, W. Yao, W.-H. Chang, and C.-K. Shih, Sci. Adv. **5**, eaax7407 (2019).